Study of the X-ray pulsar IGR J19294+1816 with NuSTAR: detection of cyclotron line and transition to accretion from the cold disc

Sergey S. Tsygankov[1,2], Victor Doroshenko[3], Alexander A. Mushtukov[4,2,5], Alexander A. Lutovinov[2], and Juri Poutanen[1,2]

[1] Department of Physics and Astronomy, FI-20014 University of Turku, Finland; e-mail: `sergey.tsygankov@utu.fi`
[2] Space Research Institute of the Russian Academy of Sciences, Profsoyuznaya Str. 84/32, Moscow 117997, Russia
[3] Institut für Astronomie und Astrophysik, Universität Tübingen, Sand 1, D-72076 Tübingen, Germany
[4] Leiden Observatory, Leiden University, NL-2300RA Leiden, the Netherlands
[5] Pulkovo Observatory of the Russian Academy of Sciences, Saint Petersburg 196140, Russia

ABSTRACT

In the work we present the results of two deep broad-band observations of the poorly studied X-ray pulsar IGR J19294+1816 obtained with the *NuSTAR* observatory. The source was observed during Type I outburst and in the quiescent state. In the bright state a cyclotron absorption line in the energy spectrum was discovered at $E_{\rm cyc}$ = 42.8 ± 0.7 keV. Spectral and timing analysis prove the ongoing accretion also during the quiescent state of the source. Based on the long-term flux evolution, particularly on the transition of the source to the bright quiescent state with luminosity around 10^{35} erg s^{-1}, we concluded that IGR J19294+1816 switched to the accretion from the 'cold' accretion disc between Type I outbursts. We also report the updated orbital period of the system.

Key words. accretion, accretion discs – magnetic fields – stars: individual: IGR J19294+1816 – X-rays: binaries

1. Introduction

Timing and spectral properties of radiation generated by accreting objects carry information about physical and geometrical properties of the systems. In the case of highly magnetized neutron stars (X-ray pulsars; XRPs) detailed analysis of the emission in different luminosity states allows us to investigate physical processes both very close to the neutron star (NS) and at the boundary between accretion disc and the magnetosphere. Moreover, observational appearance of these physical processes may drastically depend on the properties of the particular XRP (pulse period, magnetic field strength, etc.), reflecting different regimes of matter interaction with magnetic field and radiation.

Accurate knowledge of the magnetic field strength is crucial for application of physical models describing such interaction. Here we use high-quality *NuSTAR* data in order to accurately measure the magnetic field of the poorly studied transient XRP IGR J19294+1816. This information is further used to fill the gap in our knowledge of how pulsars with intermediate spin periods interact with the accretion disc. In particular, we aimed to verify our earlier prediction that there is a critical spin period (around 10 s for standard magnetic field strength) dividing all XRPs into two families: (i) short-spin pulsars able to switch to the 'propeller' regime at the final stages of their outbursts, and (ii) long-spin ones continuing to accrete stably from the 'cold' accretion disc (Tsygankov et al. 2017a). IGR J19294+1816 with ~12.4 s spin period (Rodriguez et al. 2009; Strohmayer et al. 2009) is an excellent candidate to fill the gap between these two families of XRPs.

IGR J19294+1816 was discovered by the *INTEGRAL* observatory on 2009 March 27 (Turler et al. 2009). Analysis of the archival *Swift*/XRT data of this region revealed relatively bright source showing evidence of pulsations at ~12.4 s (Rodriguez et al. 2009). The pulsar nature of the source was confirmed later by Strohmayer et al. (2009). Long-term flux variability with period of about 117.2 d was discovered by the *Swift*/BAT monitor and was associated with orbital modulation (Corbet & Krimm 2009). Based on the transient behaviour of IGR J19294+1816 and its position on the Corbet diagram an assumption about a Be/XRP nature of the source was made. The NIR spectroscopy presented by Rodes-Roca et al. (2018) directly confirmed this hypothesis resulting in the identification of the optical companion in the system with a B1Ve star located at the far edge of the Perseus arm at a distance of d = 11 ± 1 kpc.

The relative faintness of IGR J19294+1816 did not allow to make any conclusions regarding the physical properties of the NS in the system up to date. Only tentative detection of the cyclotron absorption line at ~35.5 keV was reported based on the deviation of the source spectrum from a power law at higher energies using the RXTE data (Roy et al. 2017). In this work we use long-term *Swift*/XRT monitoring observations to characterise accretion regimes in the system as well as two dedicated deep *NuSTAR* observations to describe properties of the NS in the hard X-ray range for the first time.

2. Data analysis

This work is based on the data from the XRT telescope (Burrows et al. 2005) onboard the *Neil Gehrels Swift Observatory* (Gehrels et al. 2004) obtained during monitoring programs performed during and after Type I outbursts in 2010 and 2017–2018, as well as two *NuSTAR* (Harrison et al. 2013) observations with the first one done nearly simultaneous with *Swift*/XRT in March 2018.

2.1. Swift/XRT data

High sensitivity and flexibility of the *Swift*/XRT telescope allow us to carry out long-term monitoring programs probing source flux evolution in a very broad range. Particularly, it permitted us to investigate the transition of IGR J19294+1816 from the outburst to the quiescent state. Because of the low count rates all XRT observations were performed in the Photon Counting (PC) mode and automatically reduced using the online tools (Evans et al. 2009) provided by the UK Swift Science Data Centre. [1]

Data sample consists of observations performed after Type I outbursts occurred in the end of 2010 and 2017. The corresponding light curves are shown in the top panel of Fig. 1. Luminosity was calculated from the bolometric (see below) and absorption corrected flux determined based on the results of spectral fitting in xspec package assuming absorbed power law model and distance to the source $d = 11$ kpc (Rodes-Roca et al. 2018). Taking into account low count statistics we binned the spectra in the 0.5–10 keV range to have at least 1 count per energy bin and fitted them using W-statistic (Wachter et al. 1979). [2]

In order to convert the observed 0.5–10 keV flux into the total X-ray luminosity and, correspondingly, mass accretion rate, we estimated the bolometric correction factors using two broadband *NuSTAR* observations performed in the quiescent and outburst states. Flux ratio between these two states was more than 50. As will be discussed later, the broad-band spectrum of the source depends slightly on its intensity, that is reflected in the flux-dependent bolometric correction factors. Particularly, in the quiescent state with the unabsorbed 0.5–10 keV flux around $F_{0.5-10\text{keV}} \sim 4 \times 10^{-12}$ erg s^{-1} cm^{-2} the bolometric correction (defined as the ratio of fluxes in the 0.5–100 to 0.5–10 keV ranges) was $K_{\text{bol}} \sim 1.8$, whereas during the second observation ($F_{0.5-10\text{keV}} \sim 1.1 \times 10^{-10}$ erg s^{-1} cm^{-2}) it increased up to ~ 2.5. Assuming a linear dependence of the bolometric correction on the logarithm of flux in the 0.5–10 keV band a simple equation can be obtained for $K_{\text{bol}} = 7.5 + 0.5\log(F_{0.5-10\text{keV}})$. In the following analysis we apply this correction to all XRT observations and refer to the bolometrically corrected fluxes and luminosities, unless stated otherwise.

2.2. NuSTAR data

The *NuSTAR* instruments include two co-aligned identical X-ray telescope systems allowing to focus X-ray photons in a wide energy range from 3 to 79 keV (Harrison et al. 2013). Thanks to the unprecedented sensitivity in hard X-rays, *NuSTAR* is ideally suited for the broadband spectroscopy of different types of objects, including XRPs, and searching for the cyclotron lines in their spectra.

IGR J19294+1816 has been observed with *NuSTAR* twice in March 2018 (see Table 1). First observation (ObsID 90401306002) was performed on March 3, in the very end of the orbital cycle when the source was in the lowest state ever observed. Second observation (ObsID 90401306004) occurred two weeks later, on March 16, when the source entered another regular Type I outburst. In this state IGR J19294+1816 was about 50 times brighter in comparison with the first observation.

The raw observational data were processed following the standard data reduction procedures described in *NuSTAR* user guide and the standard *NuSTAR* Data Analysis Software (nus-
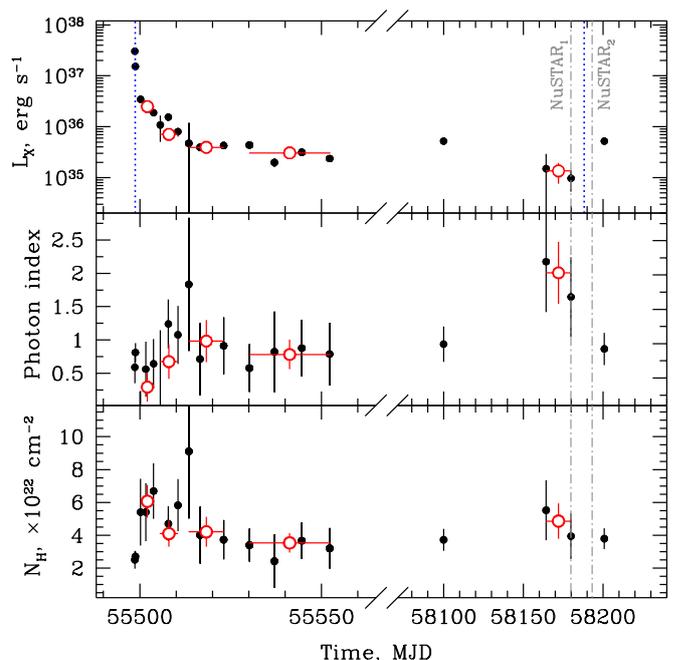
Fig. 1: *Top*: Bolometrically corrected light curve of IGR J19294+1816 obtained with the *Swift*/XRT telescope in 2010 (left side) and 2017–2018 (right side) assuming distance to the source 11 kpc. Blue dotted lines show moments of periastron passages (see Sect. 3.4). *Middle and bottom*: The corresponding evolution of the power law photon index and absorption value assuming an absorbed power law model. Black points correspond to individual XRT observations, whereas red open circles represent parameters obtained from the averaging of a few nearby observations with low count statistics. Vertical dash-dotted lines show moments of the *NuSTAR* observations.

Table 1: The *NuSTAR* observations of IGR J19294+1816.

ObsID	T_{start}, MJD	T_{stop}, MJD	Exp., ks	Net count rate, cts s^{-1}
90401306002	58179.91	58180.84	40	0.06
90401306004	58193.13	58194.06	40	2.03

tardas) v1.6.0 provided under heasoft v6.24 with the CALDB version 20180419.

The source spectra were extracted from the source-centered circular region with radius of 47″ using the nuproducts routine. The extraction radius was chosen to optimize the signal to noise ratio above 30 keV. The background was extracted from a source-free circular region with radius of 165″ in the corner of the field of view.

3. Results

The bolometrically and absorption corrected lightcurve of IGR J19294+1816 obtained with the *Swift*/XRT telescope during the monitoring programs in 2010 and 2017–2018 is shown on the top panel of Fig. 1. The overall behaviour of the source can be divided into two main states: (i) quiescent state with luminosity around 10^{35} erg s^{-1}, and (ii) outbursts associated with the periastron passage (Type I outbursts) with peak luminosity reaching $\sim 10^{37}$ erg s^{-1}. Middle and bottom panels of the figure show the corresponding evolution of the photon index and ab-

sorption value measured in the 0.5–10 keV energy band assuming absorbed power law model (PHABS × POW in XSPEC). As can be seen, this simple spectral model fits the data in XRT range at all observed flux levels. Although some spectral variability is observed, the transition to the thermal spectrum, expected in the case of cooling NS surface (see e.g., Wijnands & Degenaar 2016), is never observed in IGR J19294+1816, strongly indicating the continuation of accretion in the quiescent state.

Similar behaviour with transition of the source to the stable accretion between Type I outbursts was recently discovered in another Be/XRP GRO J1008–57 and interpreted as accretion from the cold disc (Tsygankov et al. 2017a). To study this process in more details deep broad-band observations were requested in these two states of IGR J19294+1816. In spite of only 13 days gap between observations *NuSTAR* found the source in completely different states with luminosities $L_X = 6.7 \times 10^{34}$ erg s^{-1} (ObsID 90401306002; low state) and $L_X = 3.4 \times 10^{36}$ erg s^{-1} (ObsID 90401306004; high state). The light curves of the source obtained from the *NuSTAR* data in full energy range do not reveal any strong variability. The source flux remains stable within a factor $2 - 3$ in both observations.

3.1. Pulse profile and pulsed fraction

No binary orbital parameters except orbital period are known for IGR J19294+1816. Therefore pulsations were searched in the light curves with only barycentric correction applied and resulting periods might be biased due to orbital motion of the source. Pulsations were detected with high significance in both states. The obtained count statistics of *NuSTAR* data allowed us to reconstruct pulse profiles in several energy bands from 3 to 50 keV for each observation using spin periods $P_1 = 12.4832(2)$ s and $P_2 = 12.4781(1)$ s for the low and high states, respectively (see Fig. 2). Uncertainties for the pulse periods were determined from large number of simulated light curves following procedures described in Boldin et al. (2013).

The shape of the pulse profile is very similar in different states. At the same time it demonstrates a clear dependence on energy. Below ~ 10 keV the profile has broad single peak. With the increase of energy the profile structure becomes more complicated. Particularly, it becomes double-peaked with peaks separated by 0.5 in pulsar phase.

The pulsed fraction[3] as a function of energy is shown in Fig. 3. For both states the increase of the pulsed fraction towards higher energies is observed, that is typical behaviour for the majority of XRPs (Lutovinov & Tsygankov 2009). Note that during the low state the pulsed fraction was significantly lower. Similar drop of the pulsed fraction in the low state was found in GRO J1008–57 reinforcing the similarity between these two sources.

3.2. Phase averaged spectral analysis

Discovery of the cyclotron resonance scattering feature at $\sim$ 36 keV in the spectrum of the source has been claimed by Roy et al. (2017) based on the observed deviation of the RXTE/PCA continuum from a power law above ~ 30 keV. The choice of the continuum model by the authors appears, however, to be extremely odd, because X-ray spectra of all known XRPs exhibit a cutoff above $\sim 15 - 20$ keV (see e.g., Nagase 1989; Filippova et al. 2005). The cutoff is actually expected for a spectrum pro-

---

[3] PF = $(F_{max} - F_{min})/(F_{max} + F_{min})$, where F_{max} and F_{min} are maximum and minimum fluxes in the pulse profile, respectively.
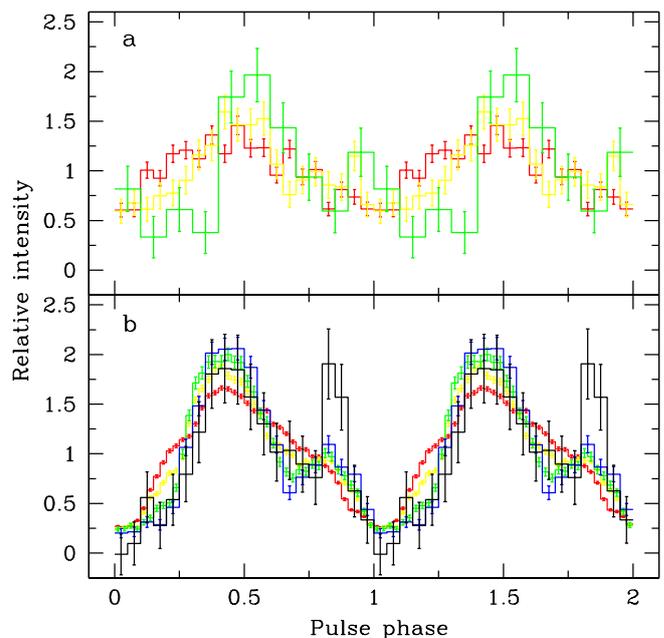

Fig. 2: Pulse profiles of IGR J19294+1816 obtained with *NuSTAR* in different energy bands during (a) low and (b) high states. Different colours correspond to different energy bands: 3–10 keV (red), 10–18 keV (yellow), 18–27 keV (green), 27–37 keV (blue), 37–50 keV (black).
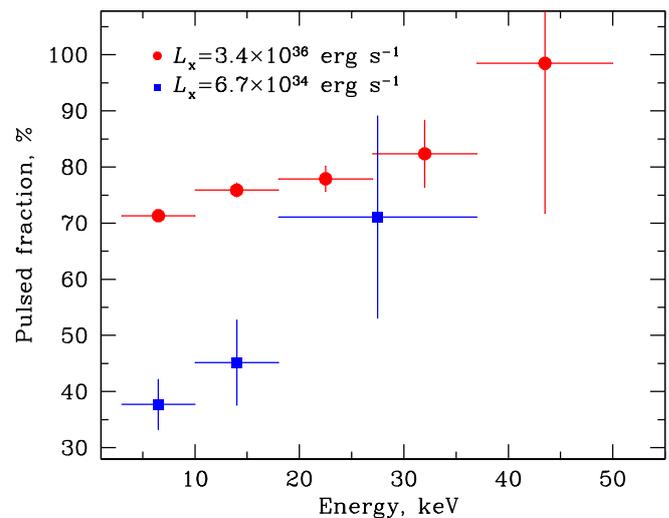

Fig. 3: Dependence of the pulsed fraction of IGR J19294+1816 on energy as seen by *NuSTAR* in the low (blue squares) and the high (red circles) states.

duced through comptonization in hot emission region (e.g. Sunyaev & Titarchuk 1980; Meszaros & Nagel 1985). It is extremely likely, therefore, that the cyclotron line included in the model in practice just mimicked the cutoff, and thus is not real.

To verify this possibility, we re-analyzed the RXTE observation 95438-01-01-00 (MJD 55499.46) where the line appeared to be most significant. Indeed, we found that the broadband RXTE/PCA continuum is perfectly well described with an absorbed cut-off power law model with no additional features required by the fit. Alternatively, it can be described with one of the comptonization models such as COMPTT or NTHCOMP with
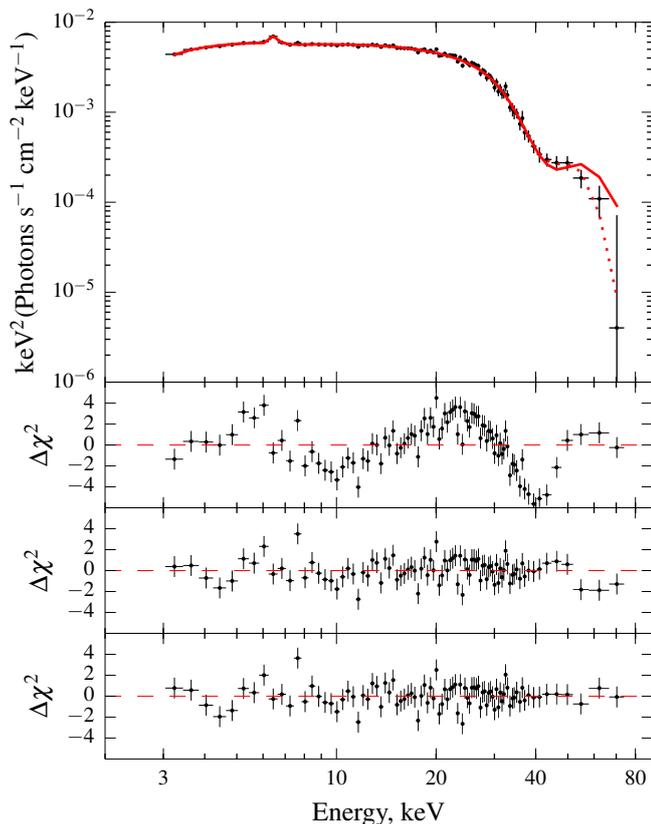
Fig. 4: Spectrum of IGR J19294+1816 obtained with the *NuS-TAR* telescopes during the high state. The data from the two *NuSTAR* units are added together for plotting (but not for actual fit). The best-fitting residuals for models (top to bottom) without inclusion of the absorption feature, with fundamental only (at ~ 42.8 keV; shown with the solid line in the top panel), and including also the harmonics (at ~ 85 keV, dotted line in the top panel) are also shown.

χ^2/dof ~ 0.8 (in all cases the fluorescence iron line was also included in the fit with the energy fixed at 6.4 keV and width at 0.1 keV). On the other hand, we verified that it is indeed possible to model the spectrum with a combination of a power law and cyclabs model, however, not only the fit quality is considerably worse in this case but also the line itself gets unreasonably deep. We conclude, therefore, that the claim of the cyclotron line discovery by Roy et al. (2017) is unsupported by the data used by the authors, which has insufficient statistics.

On the other hand, *NuSTAR* data provide much better statistics and allow us to conduct a much more sensitive search for the possible cyclotron lines in the source spectrum. Similarly to RXTE, *NuSTAR* broadband spectrum can be well described with several continuum models. However, residuals around ~ 40 keV in absorption are immediately apparent in phase-averaged spectrum from observation 90401306004 (i.e. when the source was in bright state) irrespective on the continuum model used. The fit can be greatly improved by inclusion of a gaussian absorption line in the model. The width of the line depends slightly on the continuum model, but the feature is always significantly detected at the same energy. For the nthcomp continuum model, an absorption line with energy 42.9(1) keV, width of 6.9(5) keV and optical depth at line centre of $\tau = 1.3(2)$ improves the fit from χ^2/dof = 1132/720 to χ^2/dof = 766/717, which corresponds to
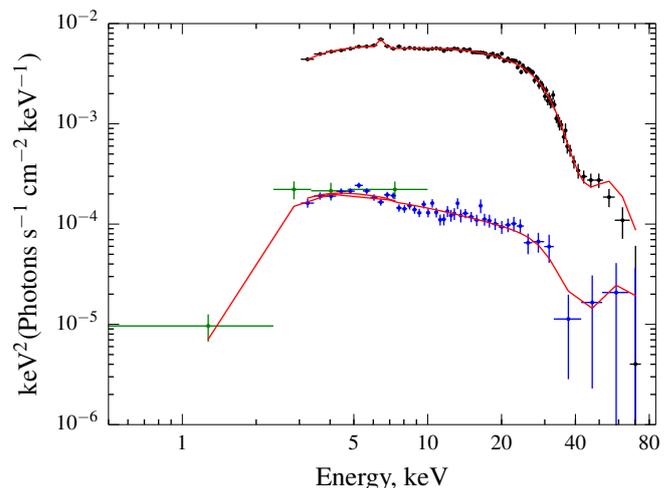
Fig. 5: Spectral energy distribution of IGR J19294+1816 obtained with the *Swift*/XRT and *NuSTAR* telescopes during the high (black dots) and low (blue and green dots) intensity states. The data from the two *NuSTAR* units are added together for plotting (but not for actual fit). Solid lines represent best-fit models for each observation including fundamental line only (see text).

probability of chance improvement of ~ 3×10^{-79} according to MLR test (Protassov et al. 2002).

The feature is, therefore, highly significant. This is also the case with other continuum models, so we conclude that while the report by Roy et al. (2017) is erroneous, the source does have indeed a cyclotron line at ~ 43 keV, which implies magnetic field of ~ 5×10^{12} G assuming gravitational redshift $z = 0.35$ for the typical NS parameters. Usage of the cyclabs model instead of gabs results in slightly lower cyclotron energy about 40 keV. Such discrepancy between these two models is associated with the definition of the latter model, and was found in other studies (e.g. Tsygankov et al. 2012; Mushtukov et al. 2015). There is also some evidence for the harmonic at double energy in the residuals (see Fig. 4), although its significance is low with false alarm probability of ~ 2% (assuming the energy and width of the fundamental fixed to be double that of the fundamental, and even lower otherwise).

The counting statistics in the second observation, unfortunately, does not allow us to confidently detect the line, nor to constrain its parameters. Constraining the luminosity-related changes of the cyclotron line energy is, however, extremely interesting given the results reported previously for other sources (Tsygankov et al. 2006; Staubert et al. 2007; Klochkov et al. 2012). We attempted thus to estimate the line energy in the low state by formally including it in the fit, and modelling the high and low-state spectra simultaneously with the absorption column and cyclotron line width and depth linked between both observations (to reduce the number of free parameters). The fit results are presented in Table 2. We found the line energy to be consistent between the observations, although uncertainties for the low-state observation are, unfortunately, rather large. It is important to emphasise, that the low counting statistics precludes significant detection of the line if only the second observation is considered. A deeper observation in quiescence would thus be required to firmly detect the line and to constrain its parameters.

Table 2: Best-fit parameters for a PHABS*NTHCOMP model obtained for both observations. For the high state observation also the absorption feature modelled as GABS and fluorescence iron line modelled as GAUSSIAN are included in the fit. Neither feature was formally required for the low state spectrum.

Parameter	Units	Low	High
$N_{\rm H}$	10^{22} cm^{-2}		6.3 ± 0.4
Γ	–	1.68 ± 0.03	$1.443^{+0.003}_{-0.006}$
$kT_{\rm e}$	keV	15^{+16}_{-4}	7.0 ± 0.2
$kT_{\rm bb}$	keV		$0.5^{\rm fixed}$
$E_{\rm Fe}$	keV	–	$6.40^{+0.07}_{-0.04}$
$\sigma_{\rm Fe}$	keV	–	$0.01^{\rm fixed}$
$N_{\rm Fe}$	10^{-5} ph cm^{-2} s^{-1}	–	6.7 ± 0.8
$E_{\rm cyc}$	keV	$41.4^{+3.0}_{-2.4}$	42.8 ± 0.7
$\sigma_{\rm cyc}$	keV		6.8 ± 0.5
$\tau_{\rm cyc}$	–		1.3 ± 0.2
χ^2/dof			1.03 (850)

Fig. 7: Spectra of IGR J19294+1816 obtained in four pulse phases shown in Fig. 6. Phase bins 1, 2, 3 and 4 correspond to red, green, blue and black points, respectively.
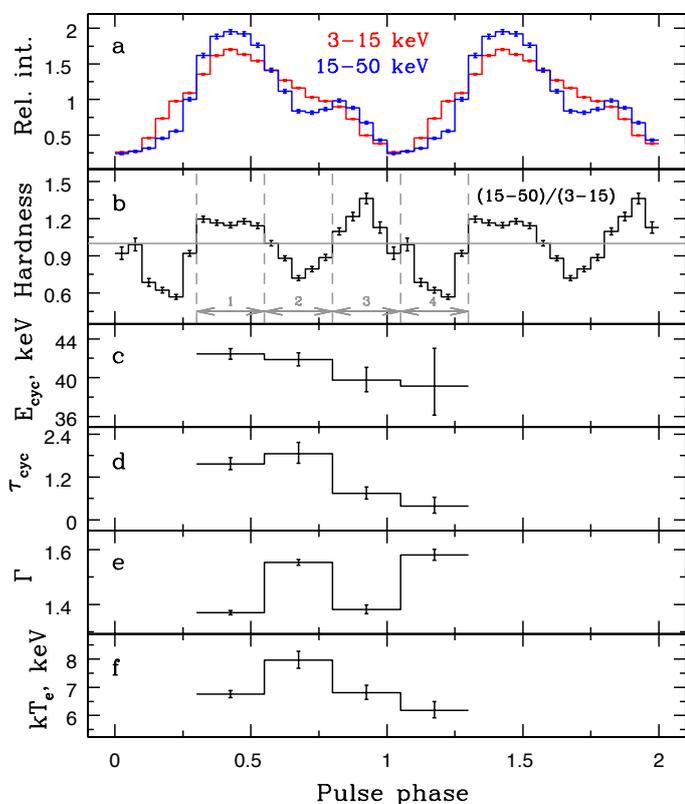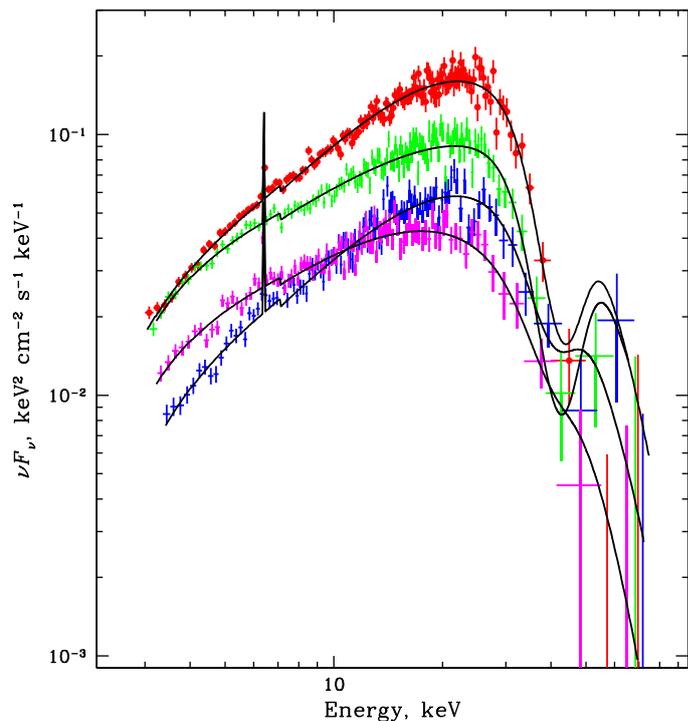

Fig. 6: Results of phase resolved spectroscopy of IGR J19294+1816 obtained with the *NuSTAR* telescope in the high intensity state.

3.3. Phase resolved spectral analysis

To investigate possible pulse phase dependence of spectral parameters in IGR J19294+1816 we performed phase resolved spectral analysis in the bright state (*NuSTAR* ObsID 90401306004). Phase bins for individual spectra were chosen based on the hardness ratio over the pulse. As can be seen from the two top panels in Fig. 6, there are four phase bins with significantly different values of hardness ratio, that can be a hint for significantly different spectral properties.

The obtained four spectra were fitted with the same model as in the case of phase averaged spectrum, i.e. PHABS*(GAU+NTHCOMP*GABS) in XSPEC. Absorption parameter $N_{\rm H}$ was free to vary and we did not find any evolution of its value over the pulse period. Because of low count statistics at high energies we froze the cyclotron line width at 6.8 keV determined from phase-averaged spectrum (see Table 2). Variability of the cyclotron line energy and optical depth is shown in Fig. 6c,d. The position of the cyclotron line does not exhibit strong dependence on the pulse phase, whereas depth of the line appears to vary significantly. In particular, the line is deepest at phases around 0.5–0.7 and is consistent with zero around phase 0.2. Parameters of the continuum (both Γ and $kT_{\rm e}$ were free to vary) are significantly different at different phases, which is in line with observed hardness variations (see Fig. 6e,f). For the illustrative purposes we show all four spectra on one plot (see Fig. 7).

3.4. Orbital period

Orbital period of the source has been estimated by Corbet & Krimm (2009) at around 117 d based on the variability of *Swift*/BAT light curve. A lot of new data has been accumulated since 2009, so we exploited that to refine the orbital period value. In particular, given the low duration and symmetric profile of the outbursts, we determined the time corresponding to the peak of each outburst in the light curve by fitting a gaussian in the light curve (for orbital cycles exhibiting any excess around the peak). These times were then used to determine the orbital period using the phase connection technique as presented in Fig. 8. The orbital period was found to be 116.93(5) d, with the outburst peak epoch of MJD 53510.9(5), which is in line with earlier estimates (Corbet & Krimm 2009; Bozzo et al. 2011).
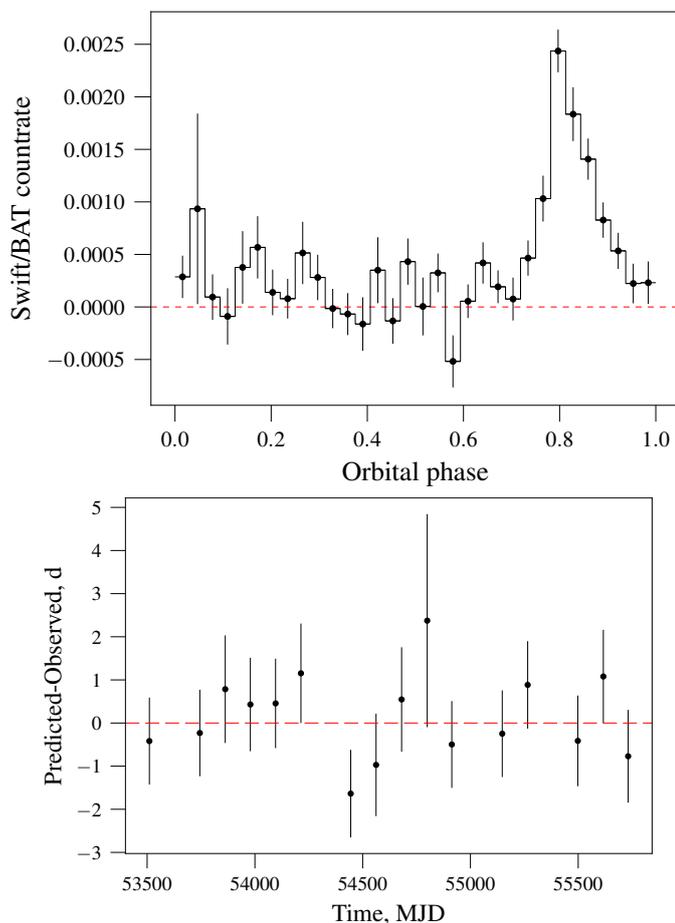
Fig. 8: *Top*: Folded light curve of the source as observed by *Swift*/BAT. The zero phase here is arbitrary to make the peak clearly visible. *Bottom*: the residuals to the linear fit of the outburst peak times determined as described in the text.

4. Discussion

One of the main goals for our observational campaign of IGR J19294+1816 was to investigate the source behaviour during its transition from the state of intensive accretion during Type I outbursts to the quiescent state between them. Particularly, transition to the propeller regime, when accretion is prohibited by the centrifugal barrier of the rotating NS magnetosphere, could be expected in the case of relatively strong magnetic field (Illarionov & Sunyaev 1975).

Observational appearance of transition to the propeller regime in classical XRP is very clear and is expressed in a sharp drop of the source luminosity by approximately two orders of magnitude, depending on the NS magnetic field (Stella et al. 1986; Tsygankov et al. 2016a,b; Lutovinov et al. 2017). A substantial softening of the energy spectrum is also expected from accretion dominated power law to the NS cooling generated black body (Tsygankov et al. 2016a). The threshold luminosity for the onset of the propeller regime is determined by the equality of the co-rotation and magnetospheric radii (see e.g., Campana et al. 2002):

$$L_{prop}(R) \simeq \frac{GM\dot{M}_{lim}}{R} \simeq 4\times10^{37} k^{7/2} B_{12}^2 P^{-7/3} M_{1.4}^{-2/3} R_6^5 \text{ erg s}^{-1}, \quad (1)$$

where P is pulsar's rotational period in seconds, B_{12} is NS magnetic field strength in units of 10^{12} G, R_6 is NS radius in units of

10^6 cm and $M_{1.4}$ is the NS mass in units of $1.4M_\odot$. The factor k relates the magnetospheric radius in the case of disc accretion to the classical Alfvén radius ($R_m = kR_A$) and is usually assumed to be $k = 0.5$, which appears justified both from theoretical and observational points of view (see e.g., Ghosh & Lamb 1979; Doroshenko et al. 2014; Campana et al. 2018).

However, recently it was shown that propeller effect can be observed only in XRPs possessing relatively short spin period and/or strong magnetic field. In the opposite case the cooling front, caused by thermal-viscous instability (see review by Lasota 2001), is able to reach inner radius of the accretion disc resulting in the NS transition to the stable accretion from the cold (low-ionization) disc before centrifugal barrier is able to fully cease accretion (Tsygankov et al. 2017a). First example of such a behaviour was recently discovered in the Be/XRP GRO J1008–57, whose spin period is ∼94 s.

Luminosity corresponding to the transition of the whole accretion disc to the cold state is determined by the inner radius of the disc and, therefore, by the strength of the NS magnetic field:

$$L_{cold} \simeq 9 \times 10^{33} k^{1.5} M_{1.4}^{0.28} R_6^{1.57} B_{12}^{0.86} \text{ erg s}^{-1}. \quad (2)$$

Below this level, the temperature in the accretion disc is lower than 6500 K at $R > R_m$ (Tsygankov et al. 2017a).

As clearly seen from Eqs. (1) and (2) the behaviour of the pulsar at low mass accretion rates is determined by the spin period of the NS and its magnetic field. Thanks to the robust determination of the NS magnetic field strength from the position of the cyclotron line we are able to apply physical models of the accretion disc interaction with magnetosphere in IGR J19294+1816. Substituting $P = 12.4$ s and $B_{12} = 5$ to Eqs. (1) and (2) one can get $L_{prop} = 2.5 \times 10^{35}$ erg s^{-1} and $L_{cold} = 0.1 \times 10^{35}$ erg s^{-1} for this source. We see that $L_{prop} > L_{cold}$, which means that the source is expected to switch to the propeller regime before the cooling wave will reach inner radius of the accretion disc causing transition to the stable accretion.

However, the observed long-term light curve of the source, shown in Fig. 1, clearly demonstrates the transition of the pulsar into stable state with luminosity around 2×10^{35} erg s^{-1} that is much higher than expected from quiescent NS in XRPs emitting its thermal energy (see e.g., Tsygankov et al. 2017b). This is clear indication that IGR J19294+1816 was able to switch to the accretion from the cold disc before the centrifugal barrier stopped the accretion.

The cold disc accretion scenario is also supported by the spectral and timing analysis. First of all, a hard power-law-like spectral shape strongly supports continuation of the accretion process. Just insignificant increase of the photon index in the low state is observed (see middle panel of Fig. 1). Also the pulsed fraction drops significantly in this state, possibly pointing to the increased emitting area. Worth noting that both mentioned features of accretion from the cold disc were observed in GRO J1008–57 (Tsygankov et al. 2017a).

The solution of this discrepancy between an expected and actual behaviour of the source can be in the proximity of IGR J19294+1816 parameters to the border between pulsars expected to transit to the propeller regime and ones able to accrete from the cold disc (see Fig. 3 from Tsygankov et al. 2017a). Therefore, substantial simplifications contained in Eqs. (1) and (2) may become important for such sources. Some of the caveats have already been discussed in Tsygankov et al. (2017a), others include neglection of the accretion torque and convection, which

might affect inner disc temperature, and thus transitional luminosity. Detailed discussion of these factors is out of scope of this paper and will be published elsewhere.

Not only Eqs. (1) and (2) are very approximate, but also the effective magnetosphere radius and thus value of k are rather uncertain (see e.g., D'Aì et al. 2015; Chashkina et al. 2017; Filippova et al. 2017; Bozzo et al. 2018). Finally, transitional luminosity level also depends on the assumed distance, which is also poorly known in most cases. It is essential, therefore, to increase the sample of objects with intermediate spin periods observed in quiescence, preferably including monitoring the transition.

5. Conclusion

In the work we present the results of the long-term observational campaign of poorly studied XRP IGR J19294+1816 performed with the *Swift*/XRT telescope as well as two deep broad-band observations obtained with the *NuSTAR* observatory. It is shown that between bright regular Type I outbursts with peak luminosity around 10^{37} erg s^{-1} the source resides in a stable state with luminosity around 10^{35} erg s^{-1}. Spectral and timing properties of IGR J19294+1816 point to the ongoing accretion in this low state, which we interpreted as accretion from the cold (low-ionization) accretion disc (Tsygankov et al. 2017a). In the bright state a cyclotron absorption line in the energy spectrum was discovered at $E_{cyc} = 42.8 \pm 0.7$ keV allowing us to estimate the NS magnetic field strength to around 5×10^{12} G. We were also able to substantially refine the orbital period of the system based on the long-term *Swift*/BAT light curve of the source.

Acknowledgements

References

Boldin, P. A., Tsygankov, S. S., & Lutovinov, A. A. 2013, Astronomy Letters, 39, 375
Bozzo, E., Ascenzi, S., Ducci, L., et al. 2018, A&A, 617, A126
Bozzo, E., Ferrigno, C., Falanga, M., & Walter, R. 2011, A&A, 531, A65
Burrows, D. N., Hill, J. E., Nousek, J. A., et al. 2005, Space Sci. Rev., 120, 165
Campana, S., Stella, L., Israel, G. L., et al. 2002, ApJ, 580, 389
Campana, S., Stella, L., Mereghetti, S., & de Martino, D. 2018, A&A, 610, A46
Chashkina, A., Abolmasov, P., & Poutanen, J. 2017, MNRAS, 470, 2799
Corbet, R. H. D. & Krimm, H. A. 2009, The Astronomer's Telegram, 2008
D'Aì, A., Di Salvo, T., Iaria, R., et al. 2015, MNRAS, 449, 4288
Doroshenko, V., Santangelo, A., Doroshenko, R., et al. 2014, A&A, 561, A96
Evans, P. A., Beardmore, A. P., Page, K. L., et al. 2009, MNRAS, 397, 1177
Filippova, E. V., Mereminskiy, I. A., Lutovinov, A. A., Molkov, S. V., & Tsygankov, S. S. 2017, Astronomy Letters, 43, 706
Filippova, E. V., Tsygankov, S. S., Lutovinov, A. A., & Sunyaev, R. A. 2005, Astronomy Letters, 31, 729
Gehrels, N., Chincarini, G., Giommi, P., et al. 2004, ApJ, 611, 1005
Ghosh, P. & Lamb, F. K. 1979, ApJ, 232, 259
Harrison, F. A., Craig, W. W., Christensen, F. E., et al. 2013, ApJ, 770, 103
Illarionov, A. F. & Sunyaev, R. A. 1975, A&A, 39, 185
Klochkov, D., Doroshenko, V., Santangelo, A., et al. 2012, A&A, 542, L28
Lasota, J.-P. 2001, New A Rev., 45, 449
Lutovinov, A. A. & Tsygankov, S. S. 2009, Astronomy Letters, 35, 433
Lutovinov, A. A., Tsygankov, S. S., Krivonos, R. A., Molkov, S. V., & Poutanen, J. 2017, ApJ, 834, 209
Meszaros, P. & Nagel, W. 1985, ApJ, 299, 138
Mushtukov, A. A., Tsygankov, S. S., Serber, A. V., Suleimanov, V. F., & Poutanen, J. 2015, MNRAS, 454, 2714
Nagase, F. 1989, PASJ, 41, 1
Protassov, R., van Dyk, D. A., Connors, A., Kashyap, V. L., & Siemiginowska, A. 2002, ApJ, 571, 545
Rodes-Roca, J. J., Bernabeu, G., Magazzù, A., Torrejón, J. M., & Solano, E. 2018, MNRAS, 476, 2110
Rodriguez, J., Tuerler, M., Chaty, S., & Tomsick, J. A. 2009, The Astronomer's Telegram, 1998
Roy, J., Choudhury, M., & Agrawal, P. C. 2017, ApJ, 848, 124
Staubert, R., Shakura, N. I., Postnov, K., et al. 2007, A&A, 465, L25
Stella, L., White, N. E., & Rosner, R. 1986, ApJ, 308, 669
Strohmayer, T., Rodriquez, J., Markwardt, C., et al. 2009, The Astronomer's Telegram, 2002
Sunyaev, R. A. & Titarchuk, L. G. 1980, A&A, 86, 121
Tsygankov, S. S., Krivonos, R. A., & Lutovinov, A. A. 2012, MNRAS, 421, 2407
Tsygankov, S. S., Lutovinov, A. A., Churazov, E. M., & Sunyaev, R. A. 2006, MNRAS, 371, 19
Tsygankov, S. S., Lutovinov, A. A., Doroshenko, V., et al. 2016a, A&A, 593, A16
Tsygankov, S. S., Mushtukov, A. A., Suleimanov, V. F., et al. 2017a, A&A, 608, A17
Tsygankov, S. S., Mushtukov, A. A., Suleimanov, V. F., & Poutanen, J. 2016b, MNRAS, 457, 1101
Tsygankov, S. S., Wijnands, R., Lutovinov, A. A., Degenaar, N., & Poutanen, J. 2017b, MNRAS, 470, 126
Turler, M., Rodriguez, J., & Ferrigno, C. 2009, The Astronomer's Telegram, 1997
Wachter, K., Leach, R., & Kellogg, E. 1979, ApJ, 230, 274
Wijnands, R. & Degenaar, N. 2016, MNRAS, 463, L46